

# Changes in microstructure and physical properties of rocks caused by artificial freeze–thaw action

Jihwan Park · Chang-Uk Hyun · Hyeong-Dong Park

Received: 27 November 2013 / Accepted: 26 May 2014 / Published online: 20 June 2014  
© Springer - Verlag GmbH & Co KG Berlin-Heidelberg 2014

**Abstract** The freeze–thaw action of water inside rocks' pores, cracks, and joints plays a dominant role in physical rock weathering where the temperature fluctuates across 0 °C. To understand this process in cold regions, artificial weathering was simulated in the laboratory. Diorite, basalt, and tuff were used as specimen, and were maintained in saturated conditions to accelerate the effect of freeze–thaw weathering. X-ray computed tomography (CT) images and scanning electron microscope (SEM) photographs were obtained to investigate changes in the inner microstructure along with repeated freeze–thaw cycles. In addition, physical properties were measured during the cycles. Particle detachment, crack initiation, and propagation and porosity increase due to volumetric expansion of water inside rocks were detected using X-ray CT and SEM. The decrease in P-wave and S-wave velocities, and in weight loss were also observed. Tuff specimens, which have low tensile strength, high porosity, and loose structure, were deteriorated rapidly, while diorite specimens on the other hand, which have high tensile strength, low porosity, and compact structure, showed relatively slight changes. The frost susceptibility of basalt specimens was found to be intermediate between tuff and diorite. The developed process for cycling and freezing set up can be useful to test the various stones in terms of frost susceptibility.

**Keywords** Frost weathering · Freeze–thaw · Scanning electron microscope · X-ray computed tomography · Artificial weathering

## Introduction

The freeze and thaw action of water inside rocks is one of the main factors for the physical weathering of rocks in cold regions, except in places where the perennial temperature is below a freezing point even in summer. As water freezes, it expands by about 9.05 % of its volume. Thus, expansion of water inside pores, cracks, and joints will act to stress the surrounding rocks on freezing, and this process causes rock deterioration in cold regions. Repeated freezing and thawing of water inside rock can cause problems in liquified natural gas (LNG) storage sites and many fields, such as building, railway, road pavement, pipeline, and stone monument preservation (Fujun et al. 2006; Grossi et al. 2007; Simonsen and Isacson 1999; Tsytoich 1975), and can affect geomorphological features in cold regions (Davis 2001). To understand these phenomena, research on the physical properties and microstructure of rocks in cold region environments is essential.

To date, the effect of the freeze–thaw phenomena in rock weathering has been discussed for a long time (Table 1). Many researchers have studied the methods for detection and quantification of rock deterioration caused by freeze–thaw action. Wiman (1963) conducted frost shattering experiments for slate, schist, granite, quartzite, and gneiss using two temperature conditions; the Icelandic type varies between  $-7$  and  $+6$  °C, and the Siberian type varies between  $-30$  and  $+15$  °C. The author measured both the weight and porosity of the samples. Lautridou and Ozouf (1982) also conducted frost shattering experiments using

---

J. Park · H.-D. Park (✉)  
Department of Energy Systems Engineering, Seoul National University, Seoul, Republic of Korea  
e-mail: hpark@snu.ac.kr

J. Park  
e-mail: atria@snu.ac.kr

C.-U. Hyun  
Korea Polar Research Institute, Incheon, Republic of Korea  
e-mail: changuk.hyun@gmail.com

two temperature regimes. The light freezing ( $-8$  to  $+20$  °C) was designed to replicate the daily freezing and thawing in polar maritime regions and the more intense and prolonged freezing ( $-8$  to  $+20$  °C) was designed to replicate the temperature in polar continental regions. Total porosity, pore size distribution, saturation coefficient, permeability, and strength were measured to study the frost susceptibility of rocks. Hall et al. (1989) developed a computer-controlled rock weathering simulator used for physical weathering studies on Antarctic rock. Matsuoka (1990) studied the freezing behavior of 47 different rock samples with different moisture conditions. The temperatures varied from  $-20$  to  $+20$  °C, measured over more than 1,000 cycles. The changes in density, porosity, tensile strength, and P-wave velocity were analyzed regularly. Nicholson and Nicholson (2000) measured weight loss, density, and rock flaws of sedimentary rocks under experimental freeze–thaw weathering. The temperature cycle varied from  $-18$  to  $+18$  °C, and it was repeated 20–80 times. Chen et al. (2004) conducted  $-18$  to  $+5$  °C freeze–thaw cycles on welded tuff samples, measuring uniaxial compressive strength, P-wave velocity, porosity, and degree of saturation in order to make observations on crack patterns. Yavuz (2010) conducted  $-20$  to  $+20$  °C freeze–thaw cycles on cubic andesite samples 50 times, measuring porosity, density, water absorption, P-wave velocity, Schmidt hardness, abrasion, and uniaxial compressive strength of rock specimens every ten cycles. In this study, the physical properties of rock specimens deteriorated as weathering progressed. Ruedrich et al. (2011) performed long-term tests (1,400 cycles) to investigate the frost resistance of building stones. Temperature cycles varied from  $-20$  to  $+20$  °C and the rock specimens are made in rectangular and cylinder shapes. Density, porosity, absorption, P-wave velocity, tensile strength, and thermal expansion behavior are measured. Bayram (2012) performed  $-20$  to  $+20$  °C freeze–thaw cycles on limestone specimens to determine the deteriorations of stones. The cycles were repeated 25 times and the following variables were measured: uniaxial strength, tensile strength, flexural strength, impact strength, modulus of elasticity, porosity, and water absorption. In addition, a statistical model was developed to predict mechanical strength loss of rock specimens, and a standardized method was suggested for evaluating the freezing and thawing durability of rock. Slab-shaped specimens were frozen at  $-18$  for 12 h and thawed at  $+32$  °C for 8 h. Loss rates were calculated every cycle and the visual changes were examined every five cycles (ASTM 2004). Specimens were frozen at  $-18$  °C for 17 h and thawed at room temperature for 7 h (ISO 2007). In addition, the microscopic damages of rocks produced during freeze–thaw cyclic tests have been investigated using a scanning electron microscope

(SEM) (Marco Castaño et al. 2010; Park et al. 2010; Wright 2000) or X-ray computed tomography (CT) (Dewanckele et al. 2010; Zhang et al. 2004). So far, there has been little research on microstructure change of rock in cold regions using SEM and X-ray CT. Ruiz de Argandoña et al. (1999) used two-dimensional X-ray CT images and analyzed them qualitatively, while Rodríguez-Rey et al. (2004) used 50 slices of X-ray CT images to analyze the change of the crack aperture quantitatively. However, both of them used normal X-ray CT equipment with 450- $\mu$ m spatial resolution, so that the width of microcracks or diameter of pores less than 30  $\mu$ m were overlooked. In this research, three dimensional micro X-ray CT images with 5- $\mu$ m spatial resolution were used to investigate the pore structures of rock specimens and to analyze them quantitatively. SEM images were also obtained to observe the change of rock specimens on a mineralogical scale.

Using an artificial weathering simulator in the laboratory, this research simulated physical weathering caused by the freeze and thaw action of water inside rock. SEM photographs and three dimensional X-ray CT images were obtained to observe changes in the inner microstructure of rock specimens, and elastic wave velocity and weight loss were also measured to observe the changes in physical properties of rock specimens as weathering progressed.

## Methodology

### Sample description

In this research, various rock specimens were used to analyze the changes in rock properties in cold environments. Diorite, basalt, and lapilli tuff were used. Diorite was sampled at Goheung County, Jeollanam-do, basalt was sampled at Cherwon County, Gangwon-do, and Lapilli tuff was sampled at Hwasun County, Jeollanam-do, Korea (Fig. 1). All the rock specimens were collected in fresh conditions without visible fractures.

Constituent minerals and the texture of rock specimens were investigated using the X-ray diffraction (XRD) method and polarized light microscopy of thin sections (Fig. 2). Diorite was observed as coarse-grained and medium-colored rock consisting of plagioclase, olivine, micas, quartz, and microcline. Although there are some inner cracks in the crystals, the grain boundaries were clear and pores were not observed. The size of the crystals varied from 0.1 to 1.0 mm; basalt consisted mainly of needle-shaped plagioclase, olivine, quartz, micas, and pyroxene, and the size of the crystals were about 0.5 mm. Irregular-shaped pores were observed around needle-shaped plagioclases; lapilli tuff was noted as fine-grained rock consisting of feldspar, quartz, micas, quartzite fragments, and basaltic fragments of various sizes

**Table 1** Previous experimental studies on freeze–thaw weathering

	Wiman (1963)	Lauridou and Ozouf (1982)	Matsuoka (1990)	Nicholson and Nicholson (2000)	Chen et al. (2004)	Yavuz (2010)	Ruedrich et al. (2011)	Bayram (2012)
Rock type	Slate, schist, granite, quartzite, gneiss	Chalk, limestone	Sedimentary, igneous, and metamorphic rocks	Sedimentary rocks	Welded tuff	Andesite	Limestone, porphyry, tuff, granite	Limestone
Temperature range (°C)	–7 to +6 –30 to +15	– 8 to +20 –28 to +20	–20 to +20	–18 to +18	–18 to +5	–20 to +20	–20 to +20	–20 to +20
Number of cycles	9 to 36	300 to 500	>1,000	20 to 80	1	50	1,400	25
Density	✓		✓	✓	✓		✓	
Porosity	✓	✓	✓	✓	✓	✓	✓	
Absorption						✓	✓	
Elastic wave velocity			P		P	P	P	
UCS		✓		✓	✓	✓		✓
Young's modulus							✓	
Tensile strength			✓		✓		✓	
Schmidt hardness						✓		

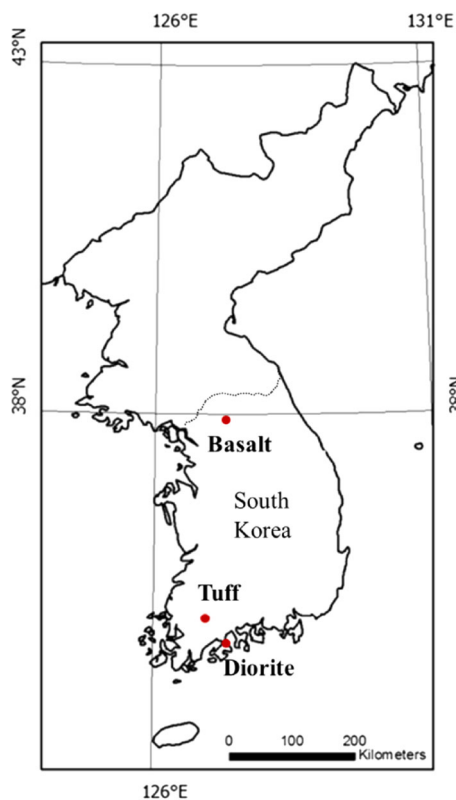


**Fig. 1** Location map of the sampling sites in Korea

and shapes. Most of the crystals were too small to observe in the microscopy image, and the quartzite and basaltic fragments were observed sparsely.

X-ray micro CT images, SEM photographs, and observations of the physical properties of rock were obtained in this research. Collected rocks were prepared in various shapes and sizes suitable for each test. The specimens for X-ray CT were prepared in cylindrical shapes with a 24.6-mm diameter and 14.5–17.7-mm length, and a 2-mm-diameter and 7-mm-deep hole was drilled at the center of the specimens. The specimens for SEM were prepared as 5 mm × 5 mm × 3 mm cubic pieces, and in total, six specimens were prepared—two for each rock type—with their observation surfaces ground down. The specimens for measuring physical properties were processed into NX-size cores with 54-mm diameters and 99.2–120.5-mm lengths. In total, six specimens were prepared—two for each rock. Using ductile coating covers made of waterproof rubber, all samples were maintained in saturated conditions during the experiments to keep the freezing–thawing effect of water inside the pores and cracks. Regarding the specimens for obtaining X-ray micro CT, the top and bottom of the specimens were blocked with stainless steel plates with a thickness of 5 mm in order to exert all of the ice pressure in parallel directions after the specimens were completely saturated and the center holes were filled with water (Fig. 3).



**Fig. 2** Thin section microscopy images of rock specimens with polars crossed ( $\times 5$ ). **a** Diorite was coarse-grained rock consisting of plagioclase, olivine, micas, quartz, and microcline. **b** Basalt consisted mainly of needle-shaped plagioclase, olivine, quartz, micas, and

pyroxene. Irregular-shaped pore were observed around plagioclases. **c** Tuff was fine-grained rock consisting of feldspar, quartz, micas, quartzite fragments, and basaltic fragments

### Experimental procedures

The SEM photographs and X-ray micro CT images were obtained, and the physical properties of rock, including elastic wave velocities and weight loss, were measured as the artificial weathering progressed. The air temperature was simulated in the laboratory and the freeze–thaw cycles were repeated from  $-20$  to  $+10$  °C. At the same time, the rates of temperature change were maintained at  $0.5$  °C per minute to prevent thermal stress, which usually occurs when the rate of temperature change is in excess of  $2$  °C per minute (Hall 1999; Hall and André 2001). Hence, thermal transmission time depends on the shape and size of the samples by setting times differently for the sample types in freeze–thaw cycles. In the case of the specimens for X-ray CT and SEM, the freezing time of the samples was less than 1 h. Thus, the holding times of maximum and minimum temperature were set to 1 h. A freeze–thaw repetition cycle takes 4 h: holding 1 h at  $-20$  °C, increasing from  $-20$  to  $+10$  °C during 1 h with temperature gradient  $0.5$  °C/min, holding 1 h at  $+10$  °C, and decreasing from  $+10$  to  $-20$  °C during 1 h with temperature gradient  $0.5$  °C/min. In the case of the NX core specimens for measuring physical properties, the freezing times of the samples were less than 4 h. Thus, the holding times of maximum and minimum temperature were also set

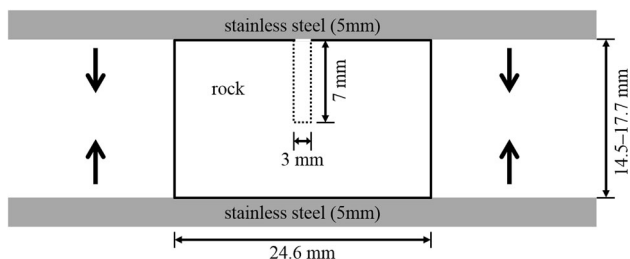


**Fig. 3** Schematic design of the specimens for X-ray CT images

to 4 h. A freeze–thaw repetition cycle takes a total of 10 h: holding 4 h at  $-20$  °C, increasing from  $-20$  to  $+10$  °C during 1 h with temperature gradient  $0.5$  °C/min, holding 4 h at  $+10$  °C, and decreasing from  $+10$  to  $-20$  °C during 1 h with temperature gradient  $0.5$  °C/min. The graphs are plotted in Fig. 4.

### Scanning electron microscope

The SEM is one of most versatile instruments available for the analysis of the microstructure morphology of rocks (Zhou and Wang 2007). In this research, SEM was used for detecting the change of pores and cracks in the rock specimens. The experiments were carried out using field emission scanning electron microscope (FE-SEM) equipment (JSM-6700F model from JEOL). The same location of each specimen was observed as weathering progressed for 150 repeated freeze–thaw cycles. The SEM photographs were obtained every ten cycles for each rock specimen until 50 cycles were reached. As there were no noticeable changes, the photographs were obtained every 25 cycles from 51 cycles until 150 cycles. Overall, the

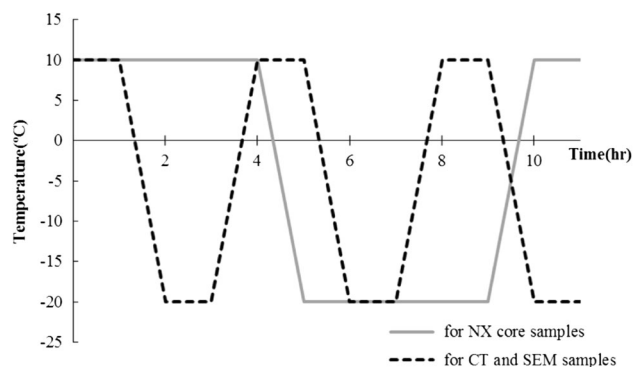
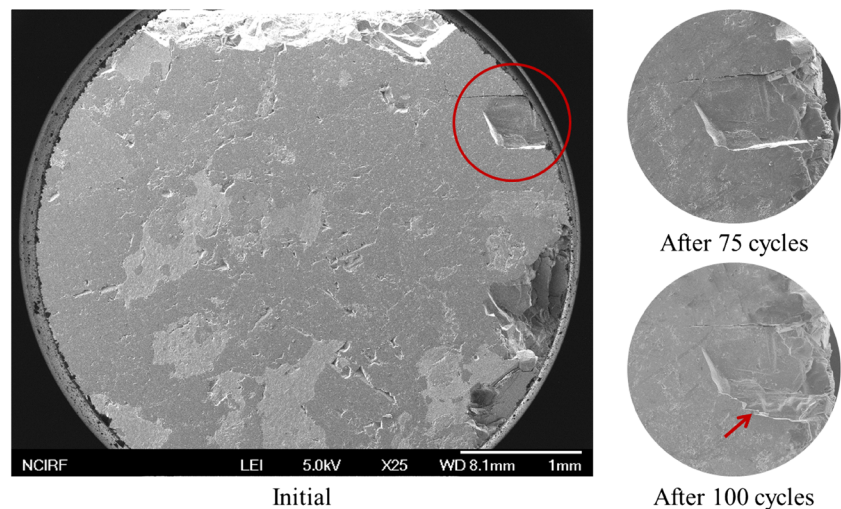


**Fig. 4** Temperature cycles used for the artificial weathering experiment

**Fig. 5** SEM photographs of a diorite specimen. A particle collapse occurred after 100 freeze–thaw cycles



SEM photographs were obtained of the initial conditions, and of conditions at 10, 20, 30, 40, 50, 75, 100, 125, and 150 cycles. To locate the occurrence of weathering, whole specimens were photographed with low-power photographs of  $\times 50$  and  $\times 150$  magnifications.

#### X-ray micro computed tomography

X-ray CT is a geometry processing technique used to generate a three-dimensional image of an object from a large number of two-dimensional, cross-sectional images. For many years, X-ray CT has been mainly used as a medical diagnostic tool, but now its use has been extended to many other fields including geological investigation, hydrology, soil science, environmental geology, petroleum geology, structural geology, sedimentology, petrology, paleontology, meteoritics, planetary science, engineering geology, and so on (Carlson 2006; Cnudde et al. 2006). Recently, micro-CT with a spatial resolution of around  $5\ \mu\text{m}$  and nano-CT with spatial resolution of around  $200\ \text{nm}$  have been developed and used in the field of geosciences. We adopted this method in our research because of its properties of non-destructivity, high accuracy, and little distortion. The CT images of three specimens—diorite, basalt and tuff—were obtained every ten freeze–thaw cycles until we reached 50 cycles. SkyScan 1,173 high-energy micro-CT with  $5\text{-}\mu\text{m}$  spatial resolution was used to detect changes in the inner structure of rock specimens under repeated freeze–thaw environment simulations. Then, pore structure was also extracted using CT images.

#### Physical properties

Measurement of P-wave and S-wave velocities of rock specimens is widely used to evaluate the physical

properties of rock because it is simple, convenient, and especially non-destructive during cycles of tests such as freeze–thaw weathering processes. In this research, P-wave and S-wave velocities were measured every ten cycles until 50 cycles for the NX core specimens of diorite, basalt, and tuff using the Pundit Lab model. Dry weight was also measured according to the methods suggested by the International Society for Rock Mechanics (ISRM) (Brown 1981).

## Results

#### Crack propagation observed from SEM images

Large-scale particle detachment was detected in diorite specimens after 100 freeze–thaw cycles (Fig. 5), and a pore connection between two adjacent pores was detected in the basalt specimens after ten cycles (Fig. 6). In the case of the tuff specimens, there were massive changes compared to the other specimens. The physical weathering was detected in the whole specimens, and the photographs of the most remarkable changes are shown in the figures. The detachment of a massive particle from the specimen occurred after 75 cycles, and a particle collapse was also detected after 100 cycles. The specimen was destroyed after 125 cycles (Fig. 7), and crack propagation and expansion were also detected. In the  $\times 150$  magnification photographs, the process of crack expansion was detected. The incomplete particle detachment occurred after 125 cycles, and the particle was seen to be completely collapsed after 150 cycles (Fig. 8). The particle collapse or detachment and pore connection were detected in all samples. In particular, the tuff specimens changed more than other specimens and one specimen was even destroyed during the course of the experiment.

**Fig. 6** SEM photographs of a basalt specimen. Pore connection caused by particle collapse was detected after ten freeze–thaw cycles

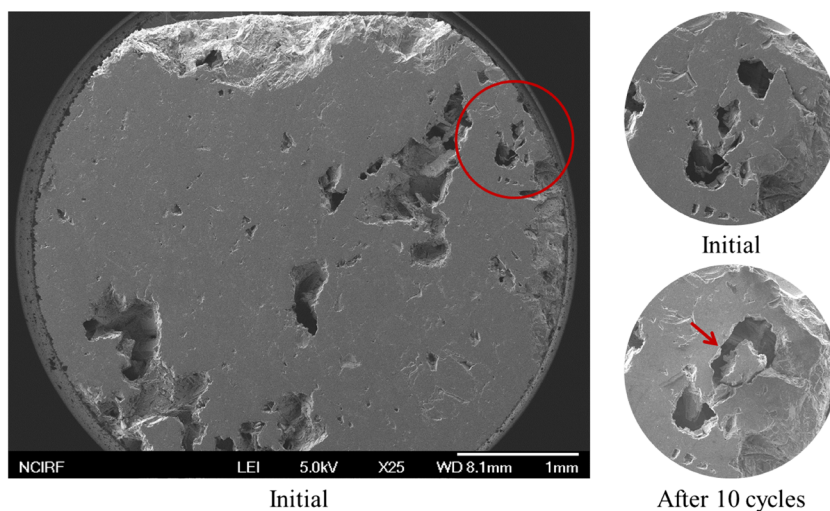


**Fig. 7** SEM photographs of a tuff specimen. Massive particle collapse was detected after 75 freeze- thaw cycles. Another particle detachment was detected after 100 cycles, and the specimen was destroyed after 125 cycles

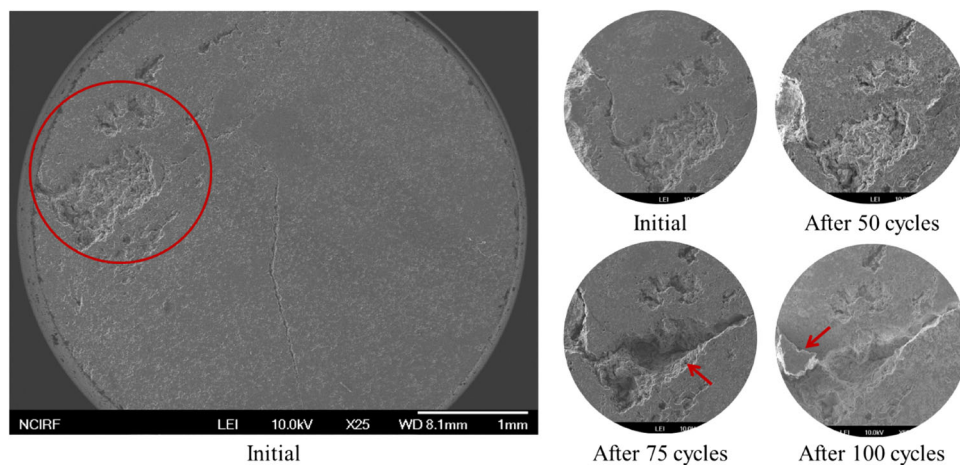
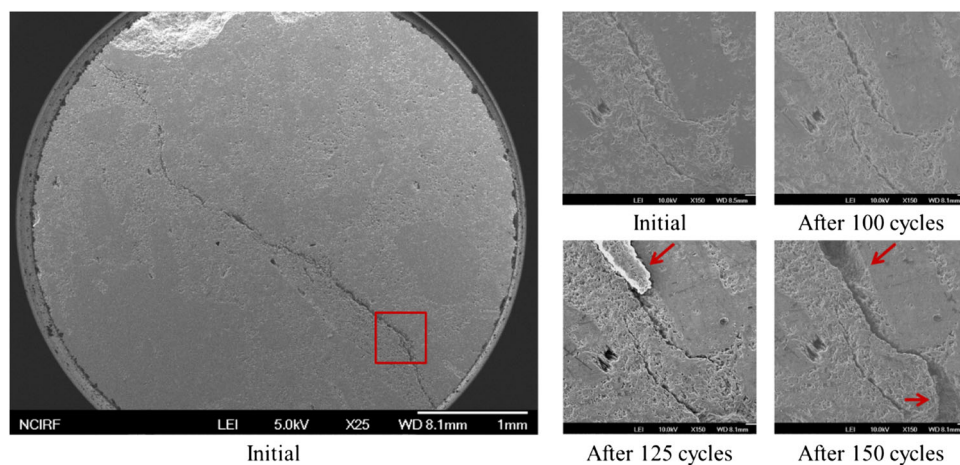


**Fig. 8** SEM photographs of a tuff specimen in which the process of crack propagation was detected. The incomplete particle detachment was detected after 125 cycles, and the crack propagation occurred after the particle was detached completely

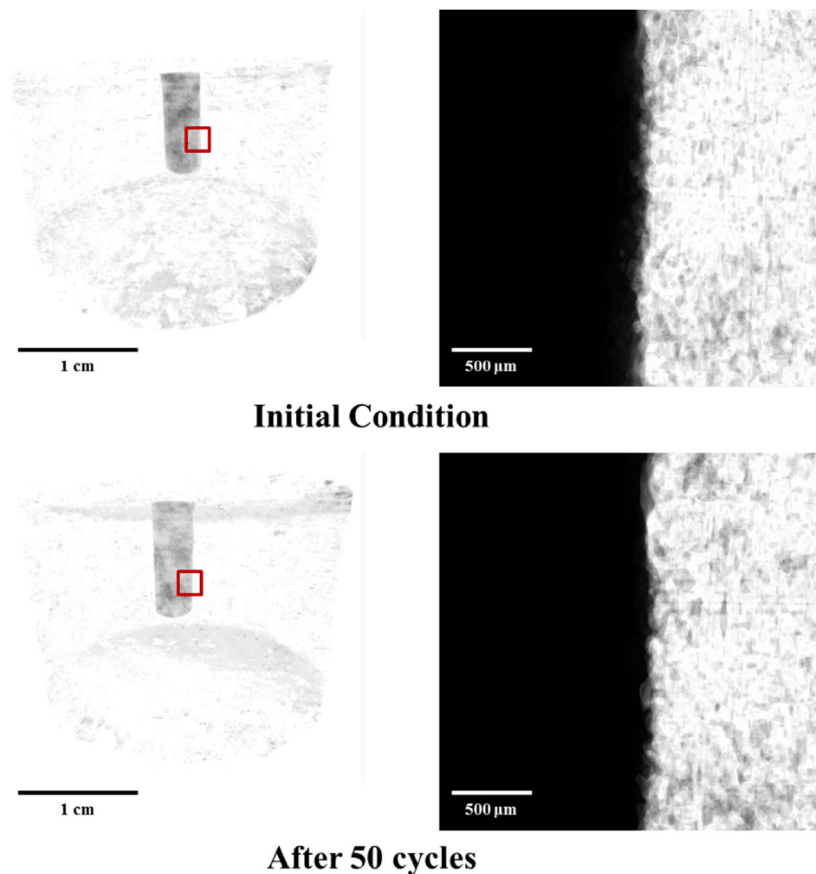


Changes in pore structures observed from X-ray computed tomography

There were no visible changes in three-dimensional CT volume renderings of the diorite and basalt specimens,

based on the results of the SEM photographs. To investigate the detailed inner structure of the specimens, the pore structure was extracted. Because the X-ray CT image was 8-bits, the images had pixel values between 0 and 255. The pixels that contained rock material were nearer

**Fig. 9** Pore structure of a diorite specimen. *Black* means pore or crack and *white* means rock specimen. There was no remarkable change



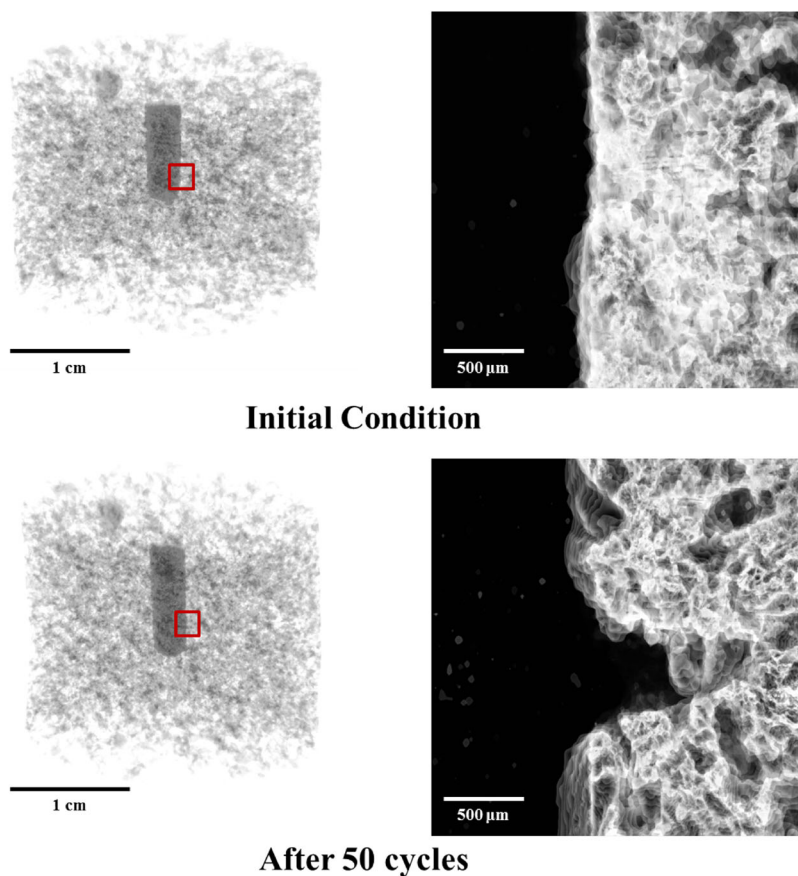
to 255, and the pixels that contained air were nearer to 0. The threshold of pore and rock was set as 6 pixels in the diorite specimens, 45 in the basalt specimens, and 15 in the tuff specimens. The pixels with an intensity lower than the threshold were assumed to be pores. After binarization was performed, pore pixels were given the value “0” and rock pixels were given the value “1”. In the images, black means a pore or crack, and white means rock. In diorite specimens, there were no remarkable changes throughout the 50 freeze–thaw cycles (Fig. 9). The images in Fig. 10 offer the pore structure of the basalt specimen, and the crack initiation and propagation detected around the hole in the center of the rock. In the three-dimensional volume-rendering images of the tuff specimen, the crack increase and expansion were detected on the surface model of CT images as weathering. In the extracted pore structure of the tuff specimen, particle detachments were detected on the whole specimen and crack initiation and propagation were detected around the hole (Fig. 11). The porosities of the specimens were extracted using the CT images (Fig. 12a). All the specimens’ porosities increased as freeze–thaw weathering progressed. The diorite specimen’s porosity increased from 0.018 to 0.025, and the

basalt specimen’s porosity increased from 0.110 to 0.122. The tuff specimen’s porosity increased rapidly compared to other specimens—from 0.094 to 0.143—which explains the most remarkable changes noted through SEM observation.

#### Changes in Physical properties

All the specimens showed the linear decrease of P-wave and S-wave velocities as freeze–thaw cycles (Fig. 12b, c), and P-wave and S-wave graphs show similar shapes. The P-wave and S-wave velocities of normal diorite are 4,500–6,500 and 3,000–3,500 km/s, respectively (Zhang 2005). The initial P-wave and S-wave velocities of the diorite specimens used in this research were about 4,762 and 3,351 m/s, respectively. After 50 freeze–thaw cycles, the P-wave and S-wave velocities decreased to 3,789 and 2,910 m/s, that is, 20.5 and 13.1 % decreases in values, respectively. The P-wave and S-wave velocities of normal basalt are 4,500–6,000 and 2,500–3,500 km/s, respectively (Zhang 2005). The initial P-wave and S-wave velocities of the basalt specimens used in this research were about 5,121 and 3,958 m/s, respectively. After 50 freeze–thaw cycles,

**Fig. 10** Pore structure of a basalt specimen. *Black* means pore or crack and *white* means rock specimen. Crack initiation and propagation were detected around the hole



the P-wave and S-wave velocities were decreased to 3,773 and 2,887 m/s, that is, 26.3 and 27.1 % decreases in values, respectively. As the P-wave and S-wave velocities of normal tuff varied in different localities, there was no standard range. The initial P-wave and S-wave velocities of the tuff specimens used in this research were about 3,590 and 2,463 m/s, respectively. After 50 freeze–thaw cycles, the P-wave and S-wave velocities were decreased to 2,409 and 1,607 m/s, that is, 32.9 and 34.8 % decreases in values, respectively. The initial P-wave and S-wave velocities show similar shapes, and higher porosities produced lower wave velocities. The dry weight of all specimens decreased linearly (Fig. 12d). The dry weight of the tuff specimens decreased 1.97 % after 50 freeze–thaw cycles, which was the biggest change among specimens. The dry weight of the diorite and basalt specimens decreased 0.26 and 0.40 %, respectively, after 50 freeze–thaw cycles.

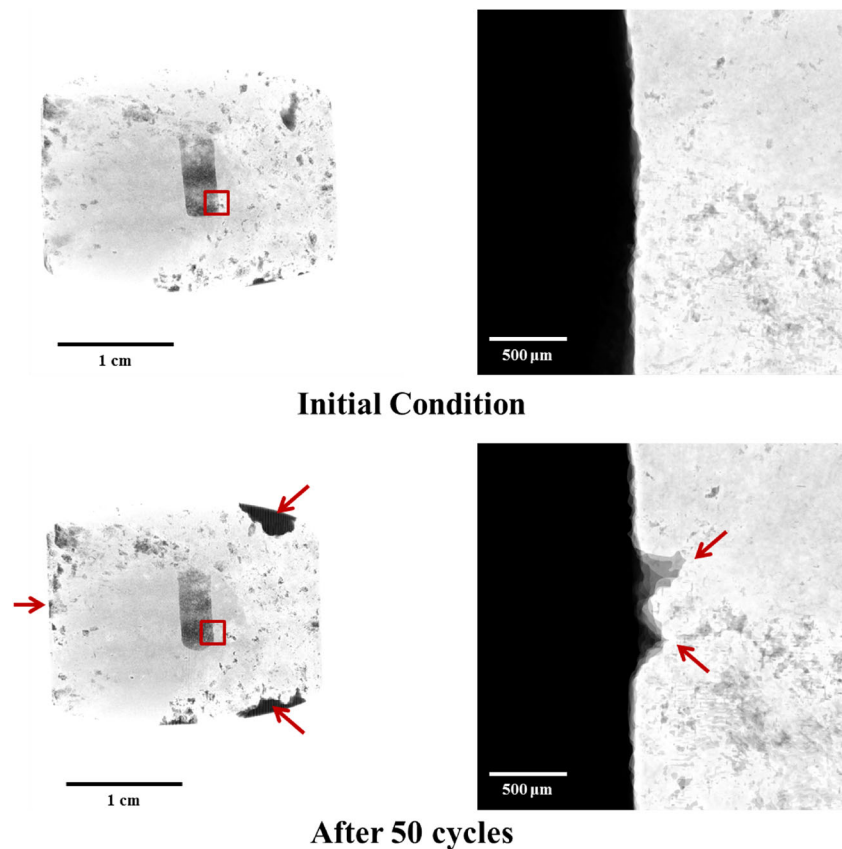
## Discussions

In the diorite specimens, there were relatively small changes because of this rock's meticulous structure, low

porosity, and high tensile strength. No remarkable changes were detected in CT images and SEM photographs, and the change of physical properties (P-wave and S-wave velocity, porosity, and dry weight) were also small compared to the other specimens. In spite of the basalt specimens' high initial porosity, there was no massive particle detachment observed in the CT images and SEM photographs because of its high tensile strength. No remarkable changes were detected in the whole sample, but the pore structure of the basalt specimen showed that the cracks were initiated and propagated around the hole. The hole in the center was a much larger space than is seen in normal pores, thus a larger-than-normal amount of water was able to expand in that space, and the pressure in the hole was greater than in normal pores. The tuff specimens with loose structures, high porosity, and low tensile strength were weakened rapidly as the freeze–thaw cycles were repeated. Particle collapse and crack initiation and expansion were detected in the SEM and CT images. The changes in the tuff's physical properties were much greater than that of the other specimens. In particular, the changes in porosity and dry weight were remarkable. The process of crack propagation was detected in the SEM images (Fig. 8). It seems that the



**Fig. 11** Pore structure of a tuff specimen. *Black* means pore or crack and *white* means rock specimen. Particle detachment and crack initiation were detected in whole of the specimen



crack expansion occurred due to repeated particle detachment around the crack.

Under optimum conditions at  $-22\text{ }^{\circ}\text{C}$ , a theoretical pressure of ice in a closed system is 207 MPa (Bland and Rolls 1998). However, this high pressure would not be reached in natural conditions for several reasons. In practice, the pressure would reach 10–100 MPa depending on the shape and roughness of the crack, the property of the rock, air or salts in cavities, and so on (Davidson and Nye 1985). Normal rock has approximately 10 MPa of tensile strength. In the case of the rock used in this research, the tensile strength of diorite, basalt, and tuff stood at 10.4, 8.8, and 5.0 MPa, respectively, using the Brazilian test suggested by the ISRM (Brown 1981). Thus, the pressure caused by water expansion inside the rock was sufficient enough to propagate the crack. The tuff specimen that had the weakest tensile strength deteriorated rapidly and significantly. Potts (1970) found that sedimentary rocks were more susceptible to freeze–thaw weathering than igneous rocks. Although tuff is classified

as igneous rock, it also has a physical structure similar to that of sedimentary rock.

There are two processes involved in freeze–thaw weathering. One is volumetric expansion and the other is ice segregation (Matsuoka and Murton 2008; Walder and Hallet 1986). The former is caused by 9 % expansion of water when it turns into ice, and the latter is caused by growth of ice lenses in the porous medium. In practice, these two processes occurred simultaneously. In repeated freeze–thaw environments, the structure of rock is weakened by the repeated volumetric expansion of water inside rock pores, cracks, and joints. In other words, rock with low tensile strength, high porosity, and loose structure is more frost-susceptible. In physical weathering of rock in cold regions, the effect of ice segregation and thermal stress is also considerable. Ice segregation is effective in bedrock fracture (Murton et al. 2006), and thermal stress or shock affects the weathering depth and produces thermal fracture in cold regions (Hall 1999). In this study, it was not clear which of these was the main process during the cycles.

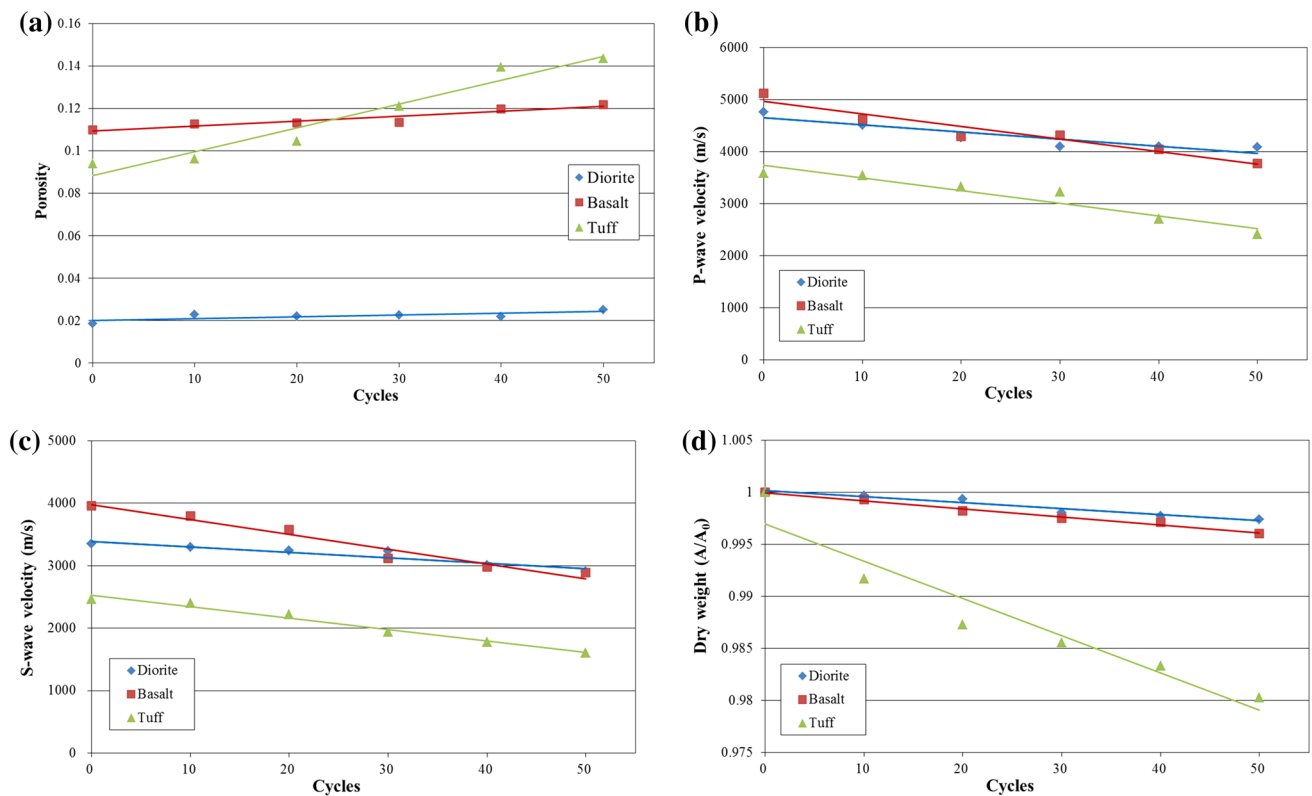


**Fig. 12** **a** Porosity changes of the specimens. All the specimens' porosities increased as freeze–thaw weathering progressed. The tuff specimen's porosity increased rapidly compared to other specimens. **b** P-wave velocity changes of rock specimens. **c** S-wave velocity

changes of rock specimens. All the specimens showed the linear decrease of P- and S-wave velocities as freeze–thaw cycles. **d** Dry weight changes of rock specimens. All the specimens showed the linear decrease of dry weight as freeze–thaw cycles

## Conclusions

Microstructural and physical properties of rock specimens were measured during artificial, repeated freeze–thaw cycles. In particular, a three-dimensional CT, non-destructive method was applied to investigate the micro-scale inner structural change of rock specimens. Using this method, changes in the same specimen can be observed continuously and can be analyzed quantitatively. Inner coring was also tried in order to exaggerate the freeze–thaw effect and to investigate crack development around the hole in greater detail. These laboratory test setups can be applied to various rocks to evaluate the frost susceptibility of various rocks.

In regions where the temperature moves around the freezing point of water, freeze–thaw weathering is dominant, and thus it is essential to understand deterioration processes of rock. This research can be applied to engineering in cold regions, including construction and maintenance of structures. Especially in areas where snow falls frequently, such as in the Nordic countries, North America, Russia, and Korea, salt is used for the de-icing of roads. The aggregates under the road are weathered due to salt crystallization and ice wedging. The test setup in this

research could be used to evaluate the degree of deterioration of the aggregates. This research can also be used to understand the decay of historical stone monuments in cold regions and to study the deterioration process in cold storage caverns for LNG, liquefied petroleum gas (LPG), frozen food, and so on.

**Acknowledgments** This work was supported by the National Research Foundation of Korea (NRF) Grant funded by the Korean government (MEST) (No. 2011-0027520).

## References

- ASTM (2004) Standard test method for evaluation of durability of rock for erosion control under freezing and thawing conditions, D 5312-04
- Bayram F (2012) Predicting mechanical strength loss of natural stones after freeze-thaw in cold regions. *Cold Reg Sci Technol* 83:98–102
- Bland W, Rolls D (1998) *Weathering: an introduction to the scientific principles*. Arnold, London
- Brown ET (1981) *Rock characterization testing & monitoring: ISRM suggested methods*. Pergamon Press, Oxford
- Carlson WD (2006) Three-dimensional imaging of earth and planetary materials. *Earth Planet Sci Lett* 249:133–147

- Chen TC, Yeung MR, Mori N (2004) Effect of water saturation on deterioration of welded tuff due to freeze-thaw action. *Cold Reg Sci Technol* 38:127–136
- Cnudde V, Masschaele B, Dierick M, Vlassenbroeck J, Van Hoorebeke L, Jacobs P (2006) Recent progress in X-ray CT as a geosciences tool. *Appl Geochem* 21:826–832
- Davidson GP, Nye JF (1985) A photoelastic study of ice pressure in rock cracks. *Cold Reg Sci Technol* 11:141–153
- Davis N (2001) *Permafrost: a guide to frozen ground in transition*. University of Alaska Press, Fairbanks
- Dewanckele J, Van Loo D, Vlassenbroeck J, Boone MN, Cnudde V, Boone MA, De Kock T, Van Hoorebeke L, Jacobs P (2010) Contributions of X-ray CT to the characterization of natural building stones and their disintegration. In: *Proceeding of the international workshop on X-ray CT for geomaterials (GeoX 2010)* vol 1, pp 164–171
- Fujun N, Guodong C, Huimin X, Lifeng M (2006) Field experiment study on effects of duct-ventilated railway embarkment on protecting the underlying permafrost. *Cold Reg Sci Technol* 45:178–192
- Grossi CM, Brimblecombe P, Harris I (2007) Predicting long term freeze-thaw risks on Europe built heritage and archaeological sites in a changing climate. *Sci Total Environ* 29:273–281
- Hall K (1999) The role of thermal stress fatigue in the breakdown of rock in cold regions. *Geomorphology* 31:47–63
- Hall K, André M (2001) New insights into rock weathering from high-frequency rock temperature data: an Antarctic study of weathering by thermal stress. *Geomorphology* 41:23–35
- Hall K, Cullis A, Morewood C (1989) Antarctic rock weathering simulations: simulator design, application and use. *Antarct Sci* 1:45–50
- ISO (2007) *Thermal-insulating materials—determination of freeze-thaw resistance*, ISO 20394-2007
- Lautridou JP, Ozouf JC (1982) Experimental frost shattering: 15 years of research at the Centre de Geomorphologie du CNRS. *Prog Phys Geogr* 6:215–232
- Marco Castaño LD, Martínez-Martínez J, Benavente D, García-del-Cura MA (2010) Failures in the standard characterization of carbonate dimension stone durability during freeze-thaw testing. In: *Proceedings of Global Stone Congress 2010*
- Matsuoka N (1990) Mechanisms of rock breakdown by frost action: an experimental approach. *Cold Reg Sci Technol* 17:253–270
- Matsuoka N, Murton J (2008) Frost weathering: recent advances and future directions. *Permafrost Periglacial Process* 19:195–210
- Murton JB, Peterson R, Ozouf J (2006) Bedrock fracture by ice segregation in cold regions. *Science* 314:1127–1129
- Nicholson DT, Nicholson FH (2000) Physical deterioration of sedimentary rocks subjected to experimental freeze-thaw weathering. *Earth Surf Process Landf* 25:1295–1307
- Park J, Hyun CU, Park HD (2010) Freeze-thaw cycle test on rocks for the simulated environment of the King Sejong Station, Antarctica. *J Korean Soc Geosys Eng* 47:731–742 (in Korean)
- Potts AS (1970) Frost action in rocks: some experimental data. *Trans Inst Br Geogr* 49:109–124
- Rodríguez-Rey A, Ruiz de Argandoña VG, Calleja L, Suárez del Río LM, Celorio C (2004) X-ray tomography characterization of microfissuration on rocks generated by freeze-thaw cycles. In: *Proceeding of the international workshop on X-ray CT for geomaterials (GeoX 2003)* vol 1, pp 293–298
- Ruedrich J, Kirchner D, Siegesmund S (2011) Physical weathering of building stones induced by freeze-thaw action: a laboratory long-term study. *Environ Earth Sci* 63:1573–1586
- Ruiz de Argandoña VG, Rodríguez Rey A, Celorio C, Suárez del Río LM, Calleja L, Llavona J (1999) Characterization by computed X-ray tomography of the evolution of the pore structure of a dolomite rock during freeze-thaw cyclic tests. *Phys Chem Earth* 24:633–637
- Simonsen E, Isacsson U (1999) Thaw weakening of pavement structures in cold regions. *Cold Reg Sci Technol* 20:135–151
- Tsyтович NA (1975) *The mechanics of frozen ground*. McGraw-Hill, New York
- Walder JS, Hallet B (1986) The physical basis of frost weathering: toward a more fundamental and unified perspective. *Arctic Alpine Res* 18:27–32
- Wiman S (1963) A preliminary study of experimental frost weathering. *Geogr Ann* 45:113–121
- Wright JS (2000) The spalling of overgrowths during experimental freeze-thaw of a quartz sandstone as a mechanism of quartz silt production. *Micron* 31:631–638
- Yavuz H (2010) Effect of freeze-thaw and thermal shock weathering on the physical and mechanical properties of an andesite stone. *Bull Eng Geol Environ* 70:187–192
- Zhang L (2005) *Engineering properties of rocks*. Elsevier, London
- Zhang S, Lai Y, Zhang X, Pu Y, Yu W (2004) Study on the damage propagation of surrounding rock from a cold-region tunnel under freeze-thaw cycle condition. *Tunn Undergr Sp Technol* 19:295–302
- Zhou W, Wang ZL (2007) *Scanning microscopy for nanotechnology*. Springer, New York